Contribution of Sialic Acid to the Voltage Dependence of Sodium Channel Gating

A Possible Electrostatic Mechanism

ERIC BENNETT, MARY S. URCAN, SALLY S. TINKLE, ADAM G. KOSZOWSKI, and SIMON R. LEVINSON

From the Department of Physiology and Programs in Neuroscience and Molecular Biology, University of Colorado Health Sciences Center, Denver, Colorado 80262

ABSTRACT A potential role for sialic acid in the voltage-dependent gating of rat skeletal muscle sodium channels (rSkM1) was investigated using Chinese hamster ovary (CHO) cells stably transfected with rSkM1. Changes in the voltage dependence of channel gating were observed after enzymatic (neuraminidase) removal of sialic acid from cells expressing rSkM1 and through the expression of rSkM1 in a sialylation-deficient cell line (*lec2*). The steady-state half-activation voltages (V_a) of channels under each condition of reduced sialylation were ~10 mV more depolarized than control channels. The voltage dependence of the time constants of channel activation and inactivation were also shifted in the same direction and by a similar magnitude. In addition, recombinant deletion of likely glycosylation sites from the rSkM1 sequence resulted in mutant channels that gated at voltages up to 10 mV more positive than wild-type channels. Thus three independent means of reducing channel sialylation show very similar effects on the voltage dependence of channel gating. Finally, steady-state activation voltages for channels subjected to reduced sialylation conditions were much less sensitive to the effects of external calcium than those measured under control conditions, indicating that sialic acid directly contributes to the negative surface potential. These results are consistent with an electrostatic mechanism by which external, negatively charged sialic acid residues on rSkM1 alter the electric field sensed by channel gating elements.

KEY WORDS: surface potential • calcium effects • glycosylation • sodium channels • voltage dependence

INTRODUCTION

Most efforts to understand how ion channels gate in response to changes in transmembrane voltages have concentrated on studies of the polypeptide structure, focusing on highly conserved motifs among ion channels that have attributes appropriate to hypothetical channel voltage sensors. For example, one such conserved structure known as "S4" consists of a repeated triad of two hydrophobic amino acids followed by a positively charged residue, consistent with a role as a voltage sensor residing within the membrane bilayer. Results from experiments using mutagenesis of the S4 region in various cation-selective channels support a role for S4 in voltage-dependent gating (Stuhmer et al., 1989; Auld et al., 1990; Papazian et al., 1991, Yang and Horn, 1995).

In addition to structural domains, the actual electric field experienced by a channel voltage-sensing mechanism is an important component of gating. Past observations suggest that the potential in the region of the channel voltage sensors is rather different than that measured experimentally using electrodes in the bulk aqueous solutions on either side of the membrane. In particular, based on the functional effects of external calcium, it has been thought that surface charges associated with the channel protein or adjacent membrane lipid phases contribute significantly to the field near a voltage sensor (e.g., Frankenhaeuser and Hodgkin, 1957; Campbell and Hille, 1976; Hahin and Campbell, 1983; see Hille, 1992). In brief, such experiments show that a greater depolarization is required to achieve a given degree of channel opening as external calcium levels are raised. To explain this effect, it was postulated that fixed negative charges on the external membrane surface are close enough to the channel that they electrostatically reduce the resting transmembrane electric field sensed by gating elements. External calcium is proposed either to bind directly to or to screen such charges, resulting in an increased local transmembrane potential that moves channels away from their macroscopic gating thresholds.

There are two possible sources for these negative surface charges: the environment surrounding the channel or the channel macromolecule itself. The first possibility was investigated in detail by Cukierman and colleagues (1988) in which the effect of the lipid environment on

Address correspondence to S.R. Levinson, Department of Physiology, C-240, University of Colorado Health Sciences Center, 4200 E. Ninth Avenue, Denver, CO 80262. Fax: 303-315-8110; E-mail: rock.levinson@uchsc.edu

the ability of external calcium to shift channel activation was studied by inserting voltage-gated sodium channels into lipid bilayers comprised of either neutral or charged lipids. These studies demonstrated that most of the calcium-induced shift was unaffected by lipid headgroup charge, and hence must depend on charges directly attached to the channel molecule. Further, Green, Weiss, and Andersen (1987*a*, *b*) observed that the conductance and toxin-binding properties of batrachotoxin-modified voltage-gated sodium channels in neutral bilayers were markedly affected by changes in external divalents and in ionic strength. These results suggested that channel-associated negative charges influence the permeability properties of sodium channels via electrostatic effects on local external surface potential. Together, these studies supply further evidence that the channel macromolecule contributes directly to a negative surface potential that affects channel function.

Biochemical characterization of purified sodium channel molecules suggests that posttranslational glycosylation of the channel may provide a significant source of these protein-associated negative surface charges. Thus a general feature of many sodium channels is that they are heavily glycosylated, with a large fraction of carbohydrate in the form of sialic acid residues that usually carry a negative charge at physiological pH. For example, the electric eel channel is comprised of 30% carbohydrate by weight, nearly 40% of which is sialic acid (Miller et al., 1983). Similar determinations have been made for muscle and brain channel carbohydrate content (Messner et al., 1985; Roberts and Barchi, 1987). The stoichiometries of sialic acid are estimated at over 100 per channel, and these charges are expected to lie on the external domain of the channel at the terminal ends of complex N-linked or O-linked glycosyl moieties. Thus we have postulated that sialic acid groups may be in part responsible for the effects of calcium on gating (Recio-Pinto et al., 1990).

In our previous studies, evidence for a such a functional role of sialic acid was obtained by comparing the gating properties of enzymatically desialylated eel electroplax sodium channels reconstituted into lipid bilayers to untreated controls (Recio-Pinto et al., 1990). The desialylated channels showed positive shifts in the voltage dependence of activation of about 30 mV, consistent with that predicted by the surface charge hypothesis. However, these studies were limited to measurement of steady-state activation properties of channels modified by batrachotoxin. Aside from the significant question of whether batrachotoxin itself could underlie an epiphenomenological shift in the gating of desialylated channels, such limited observations do not adequately address the vital issue of the mechanism of desialylation-related changes. In particular, in addition to changes in electrostatic influences, removal of large amounts of sialic acid might cause destabilization and conformational rearrangement of channel structure, leading to the functional changes observed in previous bilayer studies. So, does the negatively charged sialic acid serve to help set the electric field sensed by gating elements of the channel, or might functional consequences of desialylation instead reflect biosynthetic events involved in the folding or conformational stabilization of the channel?

To address these issues, our strategy has been to manipulate the level of sodium channel sialylation in various independent ways; we have then examined five voltage-dependent gating phenomena that are thought to be independent. In the simplest case, a surface charge hypothesis would predict that gating changes due to electrostatic influences should not depend on the manner of sialic acid manipulation and should affect all voltage-dependent processes equally.

Below we report the effects of reduced sialylation on the voltage-dependent gating of rat skeletal muscle sodium channels (rSkM1)[1] stably expressed in Chinese hamster ovary (CHO) cell lines. CHO cells were chosen for their ability to express exogenous sodium currents (West et al., 1992) and for the availability of mutant cell lines with reduced capacity to glycosylate proteins. We find that manipulations expected to decrease the amount of sialic acid on the sodium channel shifted all voltage-dependent gating parameters such that channels required a larger depolarization in order to gate. In addition, the sensitivity of channel activation to external calcium was greatly lessened under conditions of reduced sialylation. Overall, these observations are consistent with the hypothesis that channel-associated sialic acids contribute significantly to the electric field near sodium channel gating sensors.

MATERIALS AND METHODS

Preparation of Mammalian Expression Vectors Containing Wild-type and Mutant rSkM1 cDNAs

The plasmid, pZemμ1-2, was constructed from the rSkM1 clone μ1-2 (a gift of G. Mandel, S.U.N.Y., Stony Brook, NY), and the mammalian expression vector, pZem228 (Zymogenetics, Seattle, WA, a gift of Eileen Mulvihill) containing a neo selectable marker and a constitutively active metallothionine promoter, MT-1, that drives transcription of the exogenous gene.

Deletional mutagenesis was directed toward N-linked consensus sites in the first homology domain in the loop connecting pu-

[1]*Abbreviations used in this paper:* AP2944, antibody directed against an 18 amino acid sequence conserved in most voltage-gated sodium channels; CHO, Chinese hamster ovary; CHOμ1, CHO cell line stably transfected with rSkM1; rSkM1, rat skeletal muscle sodium channel 1 isoform (tetrodotoxin sensitive).

tative transmembrane segments S5 and S6 (see Fig. 10). Biochemical studies (Kraner et al., 1989) have shown that most glycosylation occurs in this region of the skeletal muscle channel, which contains eight consensus sequences for N-linked glycosylation. In the present studies, deletions were targeted to the unusual five consensus site hexad string between rSkM1 residues 291-315 (Trimmer et al., 1989). Δ1-5 and Δ2-5 deletions (removing all five or the COOH-terminal–most four sites, respectively) were made using either of two 18-mer hybrid primers. In these primers the 3′ half encoded the 3 amino acid residues (316-319) on the COOH-terminal flank of the string, while the 5′ half encoded either the flanking NH_2-terminal amino acids (288-290; Δ1-5) or the NH_2-terminal–most consensus glycosylation sequence (291-293; Δ2-5). A 1,079 bp BamHI/SplI fragment of the μ1 cDNA containing these glycosylation sites was cloned into the pSPORT1 plasmid (Gibco BRL, Gaithersburg, MD), which makes the single-stranded DNA mutagenesis template in the presence of cotransfected helper phage VCS-M13 (Stratagene Inc., La Jolla, CA). This template, generated to contain uracil using the dut^-ung^- *Escherichia coli* strain CJ236, was then subjected to "looping out" deletion mutagenesis using the primers above. Individual mutant clones were sequenced to confirm the deletions obtained, excised, and relegated back into the BamHI/SplI-digested mammalian expression vector pZemμ1-2 to yield the mutant expression plasmids.

Stable Transfection of CHO Cells and Cell Culture

CHO cells were grown to confluence in Dulbecco's Modified Eagle's Medium (GIBCO BRL) fortified with 15% FBS (Hyclone, Logan, UT), and 100 U/ml penicillin and 100 μg/ml streptomycin (GIBCO BRL) (DMEM-FBS) in a humidified incubator at 37°C and 5% CO_2, with the medium changed every 2–3 d. The cells were passed at confluence at a 1:20 dilution.

Transfections of CHO cells with the plasmid pZemμ1-2 or the vectors containing the deletional mutants described above were achieved via a calcium phosphate–mediated technique (Chen and Okayama, 1988) using 20 μg DNA and 5×10^5 cells in 10 ml of DMEM-FBS. After 24 h of incubation with DNA, standard culturing conditions were resumed. After 3 d, stably transfected cells were selected with 400 μg/ml geneticin (G418; GIBCO BRL). After the initial selection procedure of 2–3 wk, the concentration of G418 in the medium was halved. Transfected cells were grown to confluence (~3 wk) and then passaged for characterization of rSkM1 expression.

Immunocytochemistry

Site-directed polyclonal antibodies were raised to an 18-mer peptide (EOIII) corresponding to a highly conserved region (TEEQKKYYNAMKKLGSKK) in vertebrate sodium channels and were affinity purified as previously described (Dugandzija-Novakovic et al., 1995). Controls in experiments described below consisted of antibody preincubated with a 100-fold molar excess of peptide antigen.

Approximately 10,000 cells were grown overnight on a poly-L-lysine–coated glass coverslip and then fixed in a 120 mM sucrose solution containing 3.7% formaldehyde for 10 min at room temperature. Cells were permeabilized using 100% methanol at −20°C for 15 min. Nonspecific binding sites were blocked using PBS containing 20% (vol/vol) normal goat serum. The affinity purified primary antibody, AP2944 (an antibody directed against an 18 amino acid sequence conserved in most voltage-gated sodium channels), was diluted 1:100 in this blocking solution and was applied to fixed cells overnight at room temperature. The secondary antibody, fluorescein-conjugated affinity-purified goat anti–rabbit IgG, was applied for 1 h at room temperature. Cells were rinsed in PBS, mounted in Citifluor, and images obtained using the BioRad MRC-600 Laser Scanning Confocal Imaging System (Bio-Rad Laboratories, Richmond, CA) and printed on a Mitsubishi CP50U color video copy processor.

Immunoblot

CHO cells were grown in 75 cm^2 flasks to confluence, and then Dounce-homogenized in a sodium pyrophosphate buffer containing protease inhibitors (20 mM tetrasodium pyrophosphate, 20 mM Na_2PO_4, 1 mM $MgCl_2$, 0.5 mM EDTA, 300 mM sucrose, 0.8 mM benzamidine, 1 mM iodacetamide, 1.1 μM leupeptin, 0.7 μM pepstatin, 76.8 nM aprotinin). The homogenates were centrifuged at 500 *g* in a Beckman GPR centrifuge (Beckman Instruments, Inc., Fullerton, CA) for 5 min to pellet the nuclei, and the supernatants were further concentrated by spinning in a Beckman TL-100 ultracentrifuge for 1 h at 100,000 *g*. The pellets were resuspended in 250–500 μl homogenization buffer. Protein levels were determined using the Pierce BCA Protein Assay Kit (Pierce, Rockford, IL).

Samples were mixed with one volume sample buffer (10% glycerol, 5% 2-mercaptoethanol, 3% SDS, 12.5% upper Tris buffer), denatured for 2 min in boiled water, and then run on a minigel cast from 4.5% acrylamide using the discontinuous system described by Laemmli (1970). The gel was run ~90 min at 75 V and then electrophoretically transferred to nitrocellulose paper using a semi-dry transfer cell (Bio-Rad Laboratories) for 20 min at 8 V. Blots were incubated with the primary antibody overnight, followed by incubation with donkey anti–rabbit horseradish peroxidase secondary antibody (1:5,000 dilution; Amersham Corp., Arlington Heights, IL) for 2 h. Immunostaining bands were then visualized using a chemiluminescence-based kit (Renaissance; DuPont, Wilmington, DE) to expose autoradiography film (Reflection NEF; DuPont).

Whole Cell Recording of Sodium Currents in CHO Cells

Both transfected and nontransfected CHO cells were studied using the patch clamp whole cell recording technique first described by Hamill et al. (1981). Cells were passed and plated on 35 mM culture dishes for 24–96 h before the experiment.

An 8900 Dagan patch clamp amplifier with a 1 GΩ 8920 Dagan headstage was used in combination with a Nikon Diaphot inverted microscope. Pulse protocols were generated using a 486 PC computer running pCLAMP 5.0 (Axon Instruments, Foster City, CA). The resultant analogue signals were filtered at 5 kHz using an eight pole Bessel filter (9200 LPF; Frequency Devices Inc., Haverhill, MA) and then digitized at 100 kHz by the computer using a Scientific Solutions (Solon, OH) Tl-100 A/D converter interface.

Narishige micromanipulators (both mechanical and hydraulic) were used to place the electrode onto the cell. Electrode glass (capillary tubes, 2-000-210; Drummond Scientific Co., Broomall, PA) was pulled using a two step process on an electrode puller (model 720; David Kopf Instruments, Tujunga, CA) to a resistance of 1–2 MΩ measured in the salt solutions used. The external solution was (in mM) 134 NaCl, 4 KCl, 1.5 $CaCl_2$, 1.5 $MgCl_2$, 5 glucose, and 5 HEPES, while internal solution was 90 CsF, 60 CsCl, 11 NaCl, and 5 HEPES (after titration with 1 N NaOH to pH = 7.4 at room temperature). All solutions were filtered using 0.2 μm filters (Gelman Sciences, Inc., Ann Arbor, MI) immediately before use.

Effects of series resistance on the membrane potential were minimized by limiting analysis to those recordings in which uncompensated series resistance contributed less than a 2-mV error

over all voltages studied. To minimize the contribution of the endogenous current, only cells with whole cell maximal sodium currents of at least 600 pA (i.e., sixfold greater than the mean endogenous current level, see Table I) were used in the analysis.

Pharmacological and Desialylation Conditions

Inhibition studies were done using μ-conotoxin (Sigma Chemical Co., St. Louis, MO) at various concentrations continuously perfused at a rate of 0.5 ml/min through a 200 μm pipette placed ~50–100 μm from the cell. The external bath was continuously aspirated to maintain a constant level of solution in order to minimize changes in capacitive coupling in the measuring electrodes.

Enzymatic desialylation of the channels was achieved by treatment of transfected CHO cells with 75 U neuraminidase/mg cell protein (Sigma Chemical Co.) for 2 h at 37°C. Cells were passaged at least 24 h before neuraminidase treatment and were recorded from immediately after incubation with neuraminidase.

Calcium effects were studied by comparing the effects of 2.0 mM $CaCl_2$ with either 0.5 mM (*pro5* [$n = 2$], and lec2 [$n = 3$]), or 0.2 mM (CHOμ1 ± neuraminidase and Δ2-5, $n = 3$ for each) $CaCl_2$ in the external solution. In these experiments other divalents were removed, and NaCl concentration was adjusted to maintain osmolar balance. Whole cell recording of cells were made by forming seals under 2.0 mM external calcium levels, followed by perfusion of the lower level of external calcium as described above. No corrections for changes in the voltage-dependent block of sodium currents were made, as less than 7% of the sodium current was blocked under the most extreme conditions at which sodium currents were actually observed (2 mM Ca^{2+}, −30 mV). Over the more positive voltage ranges used to determine steady state or kinetic behavior, errors arising from differences in the uncorrected relief of calcium block would have been negligible (Levinson, S.R., unpublished calculations, also see Hahin and Campbell, 1983; Armstrong and Cota, 1991; Patel and Levinson, 1994).

Pulse Protocols Used in the Analysis of the Data

Conductance-voltage curve. The protocol used held the cell at −100 mV, stepping to various depolarized potentials (ranging from −60 to +100 mV in 10-mV increments) for 9 ms, and then returning to the holding potential. Consecutive steps were carried out every 1.5 s and the data were leak subtracted using the P/4 method, stepping negatively from the −100 mV holding potential. At each test potential, steady-state whole cell conductance was determined by measuring the peak current (or the steady-state current in the case of channels with inactivation removed proteolytically, see below) at that potential and dividing by the driving force (i.e., difference between the membrane potential and the observed reversal potential). The maximal conductance generated by each cell was used to normalize the data for each cell. Such data were then averaged with those from other cells, and the resultant average conductance-voltage curve was then fit via least-squares using the following Boltzmann relation:

$$\text{Fraction of total conductance} = [1 + \exp(V - V_a/Z_a)]^{-1}, \quad (1)$$

where V is the membrane potential, V_a is the voltage of half activation, and Z_a is the slope factor.

Steady-state inactivation curves. Steady-state inactivation of the channel was determined by first prepulsing the membrane to a depolarized potential for 500 ms, then stepping to the potential of peak current for 35 ms, and then returning to the −100 mV holding potential. The prepulse voltages ranged from −120 mV to +10 mV in 10-mV increments, followed by a test pulse to −10 mV. The data for each cell were fit to a single Boltzmann for the sole purpose of estimating the maximal current at infinite hyperpolarization; this value was then used to normalize the data for each cell. The normalized currents for many cells were then averaged and again fit to a single Boltzmann relationship (Eq. 1 above, solving for total current and substituting V_i and Z_i for V_a and Z_a, respectively) from which the mean V_i and Z_i values of the population were calculated.

Measurement of gating kinetics. For channels in which inactivation was intact (i.e., neuraminidase-treated and channels expressed in glycosylation-deficient cells), the activation and inactivation time constants were determined by fitting the current trace measured during a 9-ms depolarizing test pulse to the standard Hodgkin/Huxley model:

$$y = y_0 (1 - \exp[-t/\tau_m])^3 (\exp[-t/\tau_h]), \quad (2)$$

where y_0 is the peak current at the test potential, t is the time following the pulse onset, τ_m is the activation time constant, and τ_h is the inactivation time constant. To do this, τ_h and y_0 were independently determined by fitting the current decay from 80% of the measured peak current to its asymptote to a single exponential, extrapolating back to time zero. Time zero was determined by the speed of each clamp calculated from the rate of capacitive rise for a pulse from −100 to −120 mV (50–100 μs). After the determination of τ_h and y_0, the full current trace was then fit to the equation above to determine τ_m.

Measurement of Gating Kinetics in the Absence of Inactivation in rSkM1 Deletion Mutants

Analysis of voltage-dependent gating in rSkM1 mutants lacking potential glycosylation sites was done primarily in the absence of inactivation so that activation and deactivation could be measured more directly. Before inactivation removal, normal current traces were obtained for later extraction of inactivation time constants. Cells were internally perfused with papain (1 mg/ml Type X; Sigma Chemical Co.) as described (Cota and Armstrong, 1989); removal of inactivation occurred within 5–15 min. In addition, sodium levels were raised in the internal solution and lowered in the external as described (Cota and Armstrong, 1989) to increase precision of measurements over the gating ranges studied. The internal solution was (in mM) 90 NaF, 34 NaCl, 30 $CsCl_2$, 10 EGTA, and 5 HEPES (titrated to pH 7.4 with CsOH), while the external solution was 80 NaCl, 33 cholineCl, 2 $CaCl_2$, 4 KCl, 5 glucose, and 5 HEPES (titrated to pH = 7.4 with NaOH for a total sodium concentration of ~82 mM).

To determine deactivation kinetics, channels were fully activated with a pulse to +60 mV for 0.5 ms, and deactivation currents were elicited by hyperpolarizing pulses between −100 and +60 for 3.0 ms (no measurable current decay occurred at +20 or higher). Deactivation time constants were obtained by fitting the resultant currents to a single exponential decay. Activation time constants were also obtained in the absence of inactivation by using the standard activation protocol (above) and fitting the rise of current to the steady state with an exponential association raised to the third power according to the Hodgkin-Huxley formalism (Oxford, 1981), yielding τ_m and y_0. Finally, inactivation time constants for these channels were obtained by fitting the current traces obtained from the same cell before removal of inactivation, using the complete Hodgkin-Huxley model in which τ_m and y_0 were held constant. All currents were analog filtered at 50 kHz before digitizing to improve time resolution.

Data Analysis

The data were analyzed using a combination of pCLAMP 5.0 and SigmaPlot 4.0 (Jandel Scientific, Corte Madera, CA) software.

RESULTS

Biochemical Characterization of rSkM1 Stably Expressed in Chinese Hamster Ovary Cells

A mammalian expression vector containing a cDNA insert encoding rSkM1 was constructed and used to transfect the Chinese hamster ovary cell line CHO-K1 (see MATERIALS AND METHODS). Cells stably expressing the rSkM1 transcript were selected via long-term antibiotic resistance and are hereafter referred to as CHO-μ1.

It has been shown that CHO-K1 cells express low levels of an endogenous sodium current and that a neuronal channel subtype likely underlies this current (West et al., 1992; Lalik et al., 1993). We thus characterized rSkM1 expression in the transfected cells in order to assess whether endogenous channel expression was likely to contaminate exogenously expressed current. Immunocytochemical and immunoblot analysis showed that in CHOμ1, sodium channels were expressed at levels far above that observed in nontransfected cells. Thus CHOμ1 cells showed much higher levels of sodium channel immunostaining than do nontransfected cells (Fig. 1 *A*), while immunoblots indicate that there is a high level of rSkM1 expression at the protein level that greatly exceeds that of the endogenous channel protein (Fig. 1 *B*, lanes *1* and *2*). Furthermore, the endogenous channel protein appears to be significantly larger, as expected for brain versus muscle channel isoforms.

Functional Characteristics of Sodium Currents in CHOμ1

Transfected cells generally exhibit large sodium currents. These currents start to activate around −50 mV, reach their peak values around −10 mV, and reverse in accordance with the predicted sodium reversal potential (Fig. 2, *A* and *B*). Furthermore, currents activate and inactivate rapidly as in native tissue (Pappone, 1980). This is in contrast to expression of rSkM1 currents in *Xenopus* oocytes, where inactivation is observed to be much slower (Trimmer et al., 1989; Zhou et al., 1991).

Current levels ranged up to 20 nA, with an average peak current of 2.2 ± 0.14 nA (n = 126 cells). However, expression of current appeared bimodal with approximately half of the cells expressing very low or undetectable currents. This is also roughly consistent with the pattern of immunocytochemical staining, which showed considerable variation in staining intensity among individual cells (Fig. 1 *A*). The transfection is quite stable; currents were measured in CHOμ1 cells through passage 40 with no apparent decrease in the level of sodium channel expression. Finally, CHO-K1 cells transfected with only the pZem228 vector showed no significant differences in the sodium current magnitude or properties compared with nontransfected cells (data not shown).

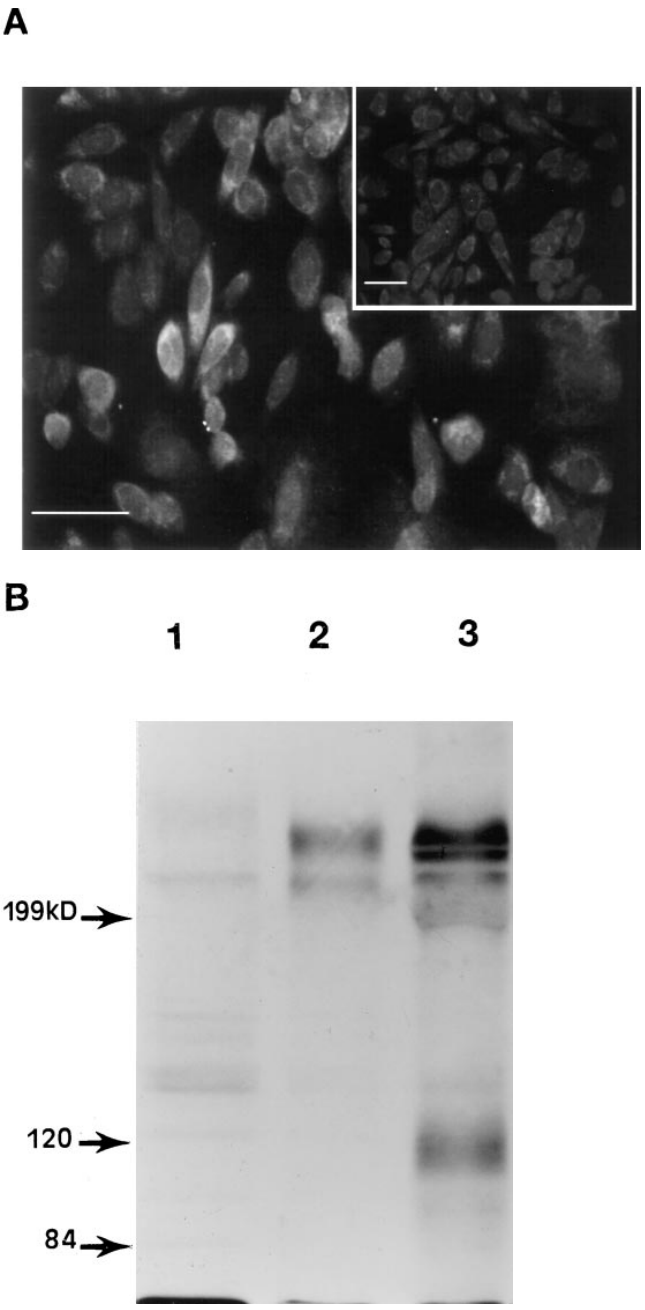

FIGURE 1. rSkM1 protein is expressed in stably transfected CHO cells. (*A*) Immunocytochemistry of sodium channels expressed in transfected and nontransfected cells. *Main photo:* transfected CHO-K1 (CHOμ1) cells; *inset:* nontransfected CHO-K1 cells. Fainter perinuclear stain of CHO-K1 cells is significant and probably reflects endogenous channels, as preincubation of AP2944 with EOIII reduced this pattern to a uniform dark background (data not shown). Scale bars = 50 μm. (*B*) Immunoblot of CHOμ1 homogenates. Lane *1*: nontransfected CHO-K1 homogenate (10 μg protein). Lane *2*: CHOμ1 homogenate (2.5 μg protein). Lane *3*: rat skeletal muscle homogenate (7 μg protein). Bands smaller than 200 kD are thought to be channel breakdown products, as these disappeared with preincubation of primary antibody with EOIII antigen (data not shown).

Endogenous currents are typically much smaller than currents in transfected cells (Fig. 2 *B*). Thus mean currents in nontransfected cells were 6% of the transfected levels in cells satisfying the recording criteria described in MATERIALS AND METHODS (90.3 ± 7.6 pA [n = 12] in CHO-K1, versus 1,501 ± 197 pA [n = 10] in CHOμ1). Moreover, the two currents differed significantly in their functional and pharmacological properties. In particular, endogenous currents gate at significantly more positive potentials than rSkM1-related currents (Fig. 2, *B–D*). In addition, exogenous currents were characterized by their high degree of sensitivity to μ-conotoxin, which is selective for skeletal muscle sodium channels of the tetrodotoxin-sensitive phenotype (Moczydlowski et al., 1986). As predicted, sodium currents in CHOμ1 cells were almost completely inhibited by sub-μM concentrations of toxin (Fig. 3), whereas the endogenous currents seen in nontransfected CHO cells were completely unaffected by μ-conotoxin concentrations up to 1 μM (data not shown). Overall, the contribution of endogenous neuronal phenotype currents was effectively minimized simply by choosing transfected cells expressing sufficiently large currents for our experiments (see MATERIALS AND METHODS).

Enzymatically Desialylated Channels Gate at More Positive Potentials

In purified preparations, channel sialylation can be reduced through exposure to the enzyme neuraminidase (Roberts and Barchi, 1987; Gordon et al., 1988; Recio-Pinto et al., 1990; Ivey et al., 1991). As a first test of the effect of sialylation on rSkM1 function, CHOμ1 cells were treated with neuraminidase (MATERIALS AND METHODS).

To assess whether the above manipulations indeed affected sodium channel sialylation, immunoblot analysis of CHO cell extracts was performed. Neuraminidase treatment caused sodium channel immunoreactivity on western blot to migrate as a broader band at a lower mean apparent molecular weight (M_r) than untreated CHO-μ1 cells, consistent with the enzymatic removal of sialic acid from channel protein (Fig. 4 *A*, *inset*). The average M_r shift was 4.7 ± 1.1 k (n = 5), indicative of a loss of ~15–20 sialyl residues (see DISCUSSION).

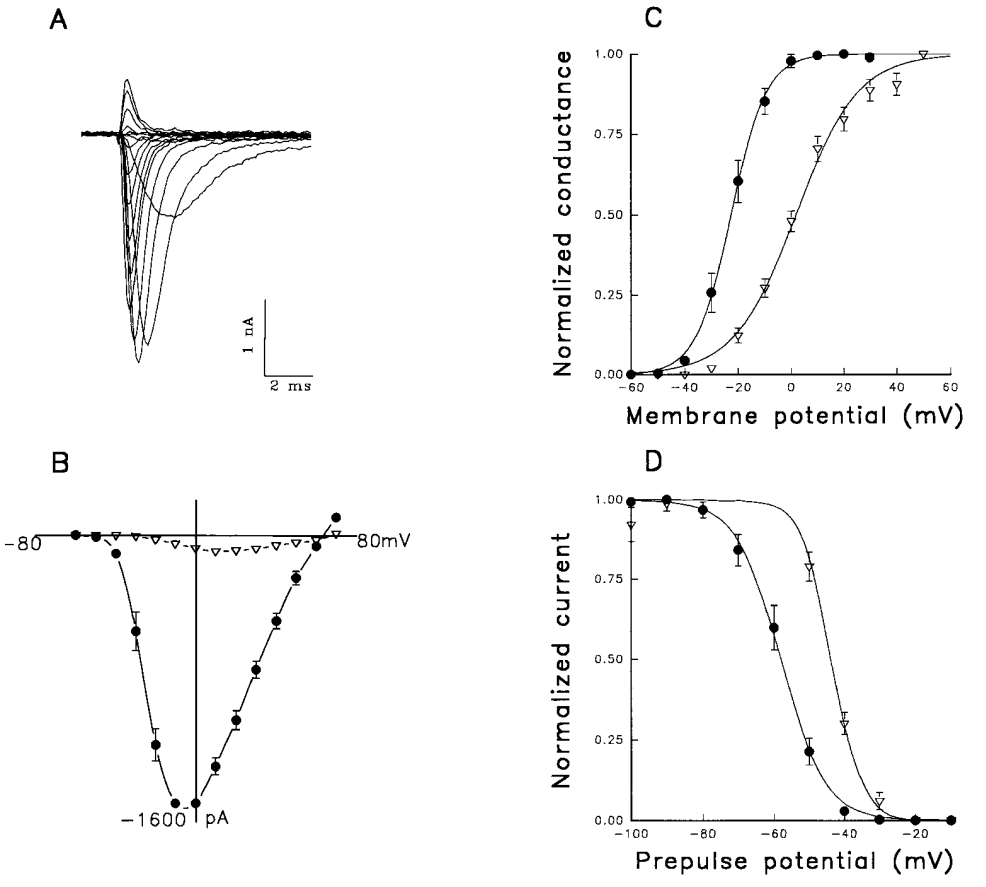

FIGURE 2. rSkM1-transfected CHO cells express large sodium currents that differ from small endogenous currents. (*A*) Current trace from a cell transfected with rSkM1 (CHOμ1). Currents were elicited by a 9-ms depolarizing pulse to potentials ranging from −60 to +100 mV in 10-mV intervals from the −100 mV holding potential. (*B*) Whole-cell sodium current-voltage relationship for transfected and nontransfected CHO-K1 cells. Points represent the average current ± SEM at a test potential. *Filled circles:* transfected CHOμ1 cells (n = 10). *Open triangles:* nontransfected CHO-K1 (n = 12). Curves are nontheoretical, point to point lines. (*C*) Conductance-voltage relationship. Data are the average peak conductances ± SEM at a membrane potential. Curves are fits of the data to single Boltzmann distributions. *Filled circles:* transfected CHOμ1 cells (n = 10). *Open triangles:* nontransfected CHO-K1 cells (n = 12). (*D*) Steady-state inactivation. Data are the average normalized current ± SEM measured during a 35-ms pulse to −10 mV following a 500-ms prepulse to the potentials graphed. Curves are fits of the data to single Boltzmann distributions. *Filled circles:* transfected CHOμ1 cells (n = 8). *Open triangles:* nontransfected CHO-K1 cells (n = 8).

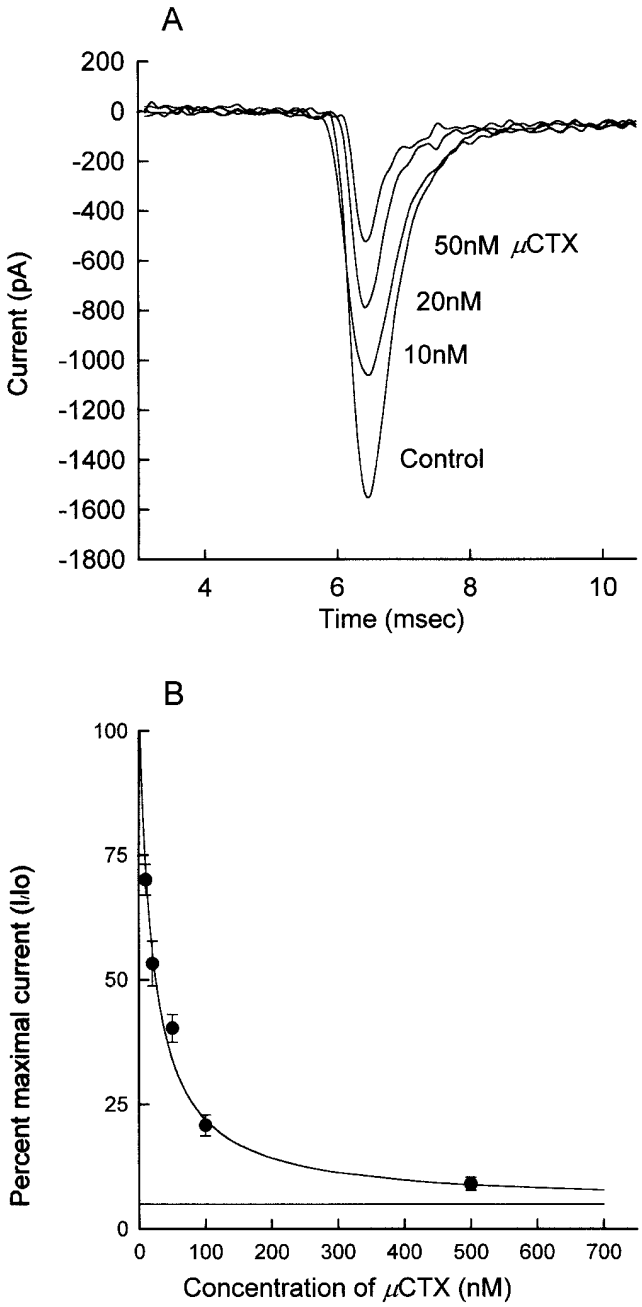

FIGURE 3. Sodium currents in rSkM1-transfected CHO cells are μ-conotoxin sensitive. (*A*) Effect of μ-conotoxin on sodium currents expressed in CHOμ1. Currents were elicited by a 9-ms pulse to −10 mV from the −100 mV holding potential. (*B*) Concentration dependence of μ-conotoxin inhibition of CHOμ1 sodium currents. Data are the average peak currents ± SEM elicited by a −10-mV test pulse, normalized to the current observed at zero toxin concentration (n = 4–5 at each concentration). Curve is a fit of the data to the equation:

$$\%\ \text{max. current} = 100 \cdot K_d / (K_d + [\mu\text{-conotoxin}]),$$

where K_d is the dissociation constant for μ-conotoxin, calculated to be 20.4 nM. The horizontal line is the average level of μ-conotoxin insensitive endogenous current (6% of the average peak current).

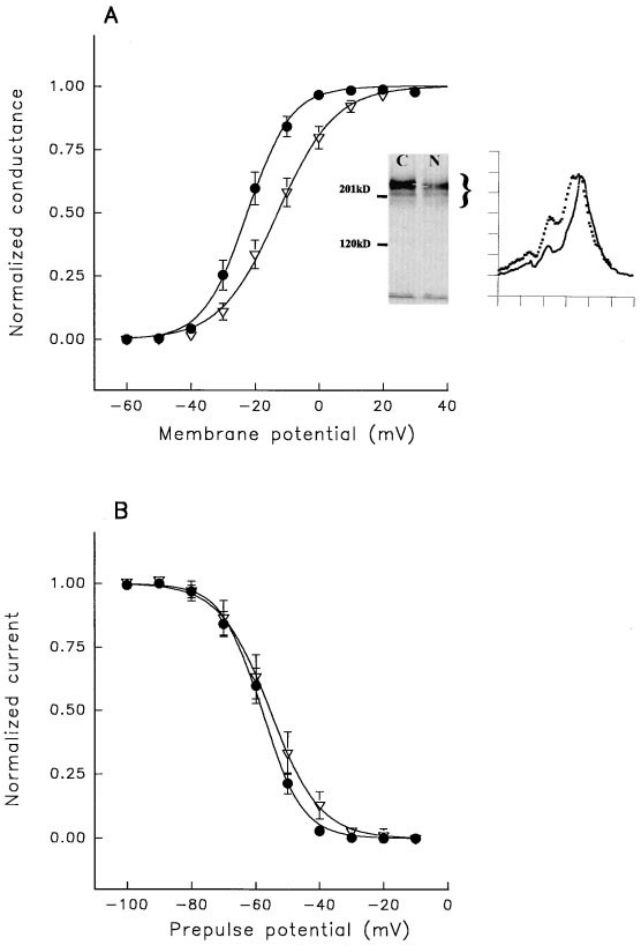

FIGURE 4. Neuraminidase treatment affects steady-state gating of rSkM1 in CHOμ1 cells. *Filled circles:* control (untreated) currents; *open triangles:* currents following neuraminidase treatment. Points are means ± SEM. Curves are fits of the data to single Boltzmann distributions. Data were collected and analyzed as described in Fig. 2 and in MATERIALS AND METHODS. (*A*) G-V relationship (n = 10 for both control and neuraminidase-treated groups). *Inset* (*left*): Western blot of cell homogenates from untreated control cells (*C*) and neuraminidase-treated cells (*N*). White marker lines show positions of peak density of major bands for comparison. *Inset* (*right*): Densitometric scans of major bands (*bracket on blot*) of untreated (*solid trace*) and neuraminidase-treated homogenates (*broken trace*). Data from both traces were scaled to allow better comparison of band mobilities. (*B*) Steady state inactivation (n = 10 for control, n = 8 for neuraminidase-treated groups).

Steady-state activation and inactivation were determined to evaluate the effects of enzyme treatment on the voltage dependence of channel gating. Neuraminidase treatment shifted the conductance-voltage curve by about 10 mV in a depolarizing direction, as measured from the change in the activation midpoint potential (V_a) relative to untreated cells (Fig. 4 *A*, Table I). Changes in steady-state inactivation were in the same direction, although of lesser magnitude (Fig. 4 *B*, Table I). In addition, neuraminidase-treatment also

shifted the voltage dependence of gating kinetics toward positive potentials by ~7 mV (Fig. 5), resulting in rates of activation and inactivation of treated channels that were slower at a given membrane potential than those measured under control conditions.

rSkM1 Channels Expressed in a Sialylation-deficient Cell Line Also Gate at More Positive Potentials

As a further test of the role of sialylation in channel gating, rSkM1 was transfected into a sialylation-deficient mutant CHO cell line, *lec2. lec2* cells show greatly reduced levels of CMP-sialic acid transport, the process responsible for carrying CMP-sialic acid into *trans* Golgi compartments, resulting in sharply diminished sialylation of glycoproteins (Stanley, 1985; 1989). As a control for these experiments, rSkM1 was also stably transfected into the *pro5* parental line from which *lec2* was originally isolated (although the functional characteristics of rSkM1 in *pro5* were very similar to those seen in CHO-μ1, see Table I). Immunoblot analysis of rSkM1 in *lec2* were inconclusive, as the overall levels of rSkM1 in the parent *pro5* line were too low to allow unequivocal detection above the background of neuronal type endogenous channels.

As with enzymatic reduction of sialylation, the voltage dependence of both steady-state and kinetic gating properties of rSkM1 channels in *lec2* cells changed in a depolarized direction relative to the fully glycosylated *pro5* line (Figs. 6 and 7; Table I). Furthermore, the magnitude of such shifts followed closely those measured in neuraminidase-treated cells. Thus two different methods of reducing general cell surface sialylation result in qualitatively and quantitatively similar changes in sodium channel gating.

The Voltage of Activation Is Less Sensitive to External Calcium under Conditions of Reduced Sialylation

The ability of divalent cations to shift the voltage dependence of ion channel gating has been interpreted as an indicator of the existence of negative membrane surface charges near channel gating elements (Frankenhaeuser and Hodgkin, 1957; Campbell and Hille 1976; Hahin and Campbell, 1983; see Hille, 1992). If sialic acid residues play such a surface charge role, then a predicted consequence of the reduction of sialylation would be a smaller effect of changes in external calcium concentration on the voltage dependence of channel gating. Whole cell currents from rSkM1-transfected CHO cells were measured at two different calcium levels to assess the relative effects of calcium on steady-state activation of sodium currents. In these experiments a reduction in physiological calcium (2.0 to 0.2 or 0.5 mM) was used. This was because rSkM1 gating in CHO cells is highly sensitive to shift by external calcium, and the effect is already near saturation at 2.0 mM calcium (Patel, 1994; Patel and Levinson, 1994).

Fig. 8 shows the conductance-voltage plots for channels under normal and reduced sialylation conditions at two different calcium concentrations. In both sets of experiments, activation of the desialylated channels show much smaller (approximately threefold less, $P < 0.01$) shifts due to alteration of external calcium than that observed for normally sialylated controls.

Removal of Potential Glycosylation Sites via Mutagenesis Results in rSkM1 Gating at More Positive Potentials

While immunoblot analysis suggested that the above manipulations resulted in reduced rSkM1 sialylation, in these experiments it was not possible to distinguish effects on channel gating that might have resulted from the reduced sialylation of nonchannel components. For example, sialylation of membrane glycolipids might have similarly been reduced under the above conditions, possibly resulting in general changes in membrane surface potentials or physicochemical alterations to the bulk membrane environment that could have affected rSkM1 function. To investigate this possibility, two different mutant rSkM1 channels were constructed

TABLE 1

Comparison of the Steady-state Parameters for All Cell Types Described

Cell line	No. of cells	V_a	Z_a	V_i	Z_i
		mV	*mV*	*mV*	*mV*
Nontransfected CHO-K1	12	+2.27 ± 1.83§	−11.47 ± 0.95§	−43.61± 0.84§	4.33 ± 0.52‡
CHOμ1	10	−22.05 ± 1.87	−5.85 ± 0.45	−58.42 ± 1.85	5.68 ± 0.36
Neuraminidase-treated CHOμ1	10	−12.89 ± 2.22§	−7.8 ± 0.26§	−56.56 ± 2.75*	6.27 ± 0.63*
Transfected *pro5*	11	−20.96 ± 1.77	−6.14 ± 0.21	−58.84 ± 1.21	5.04 ± 0.15
Transfected *lec2*	10	−9.65 ± 2.19§	−7.84 ± 0.42§	−53.38 ± 0.71‡	5.16 ± 0.56*
Δ1-5	10	−15.64 ± 1.14§	−6.86 ± 0.28‡	−55.79 ± 2.92*	5.03 ± 0.2‡
Δ2-5	9	−13.73 ± 1.65§	6.52 ± 0.22‡	−51.04 ± 1.17§	4.39 ± 0.27§

Values are the mean ± SEM of the parameters described for each cell line. Sialic acid–deficient cell lines were compared with parental or control lines; deletion mutants were compared with CHOμ1 to test significance as follows: *not significant ($P > 0.05$); ‡significant ($P < 0.05$); §highly significant ($P < 0.01$).

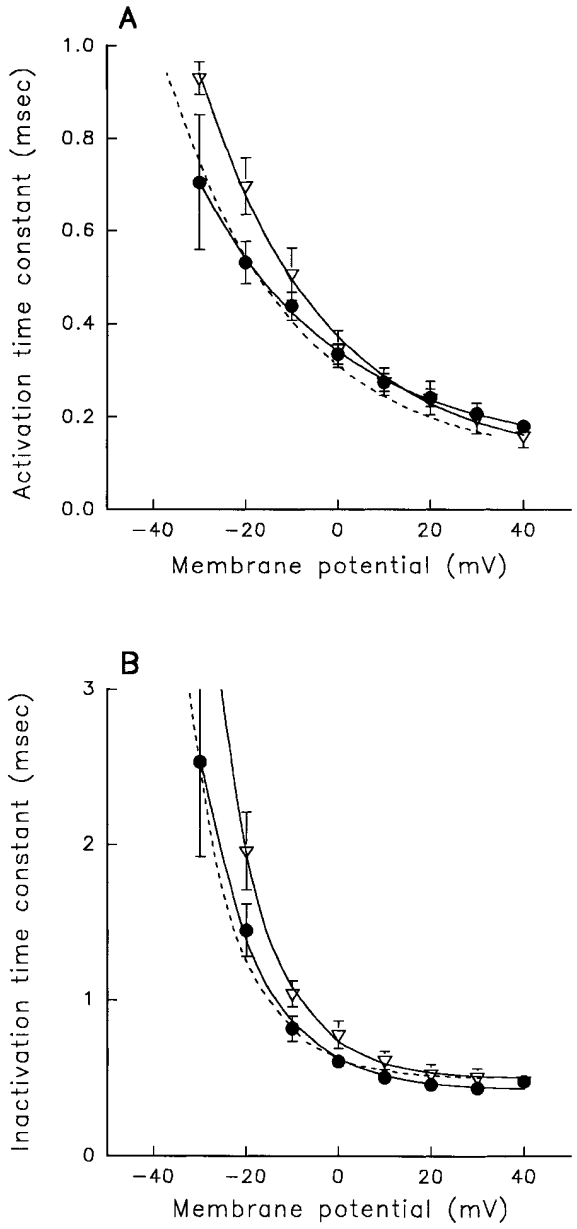

FIGURE 5. Kinetic gating behavior of rSkM1 is altered by treatment of CHOμ1 cells with neuraminidase. *Filled circles:* control (untreated) currents; *open triangles:* currents following neuraminidase treatment. Points are means ± SEM. Curves are fits of the data to single exponential functions. Time constants were measured as described in MATERIALS AND METHODS. (*A*) Time constants of activation for rSkM1 expressed in CHOμ1 cells ± neuraminidase treatment. Broken line shows fit of activation time constants for neuraminidase-treated channels following a −7-mV shift along the voltage axis ($n = 6$ for both control and neuraminidase-treated groups). (*B*) Time constants of inactivation for rSkM1 expressed in CHOμ1 cells ± neuraminidase treatment. Broken line shows fit of inactivation time constants for neuraminidase-treated channels following a −7-mV shift along the voltage axis ($n = 6$ for both control and neuraminidase-treated groups).

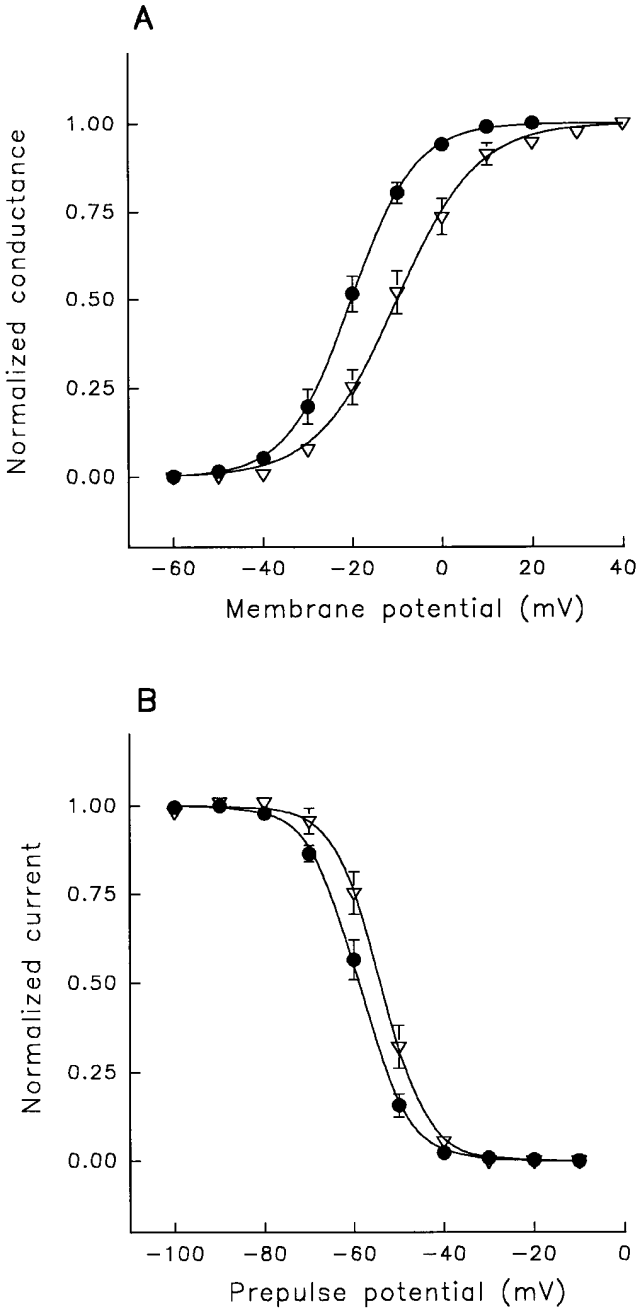

FIGURE 6. Steady-state gating of rSkM1 is altered in the sialylation-deficient CHO *lec2* cell line. *Filled circles:* parent (wild-type) *pro5* rSkM1 currents; *open triangles: lec2* rSkM1 currents. Points are means ± SEM. Data were obtained and analyzed as described in Fig. 2. (*A*) G-V relationship ($n = 11$ for *pro5*, $n = 10$ for *lec2*). (*B*) Steady-state inactivation ($n = 9$ for *pro5*, $n = 12$ for *lec2*).

in which potential N-linked glycosylation sites were eliminated (Fig. 9; see MATERIALS AND METHODS). Western blot analysis of these mutant rSkM1 channel proteins showed both mature and biosynthetic intermediate bands whose M_r values were decreased by 10k and 21k relative to the corresponding bands of the wild-

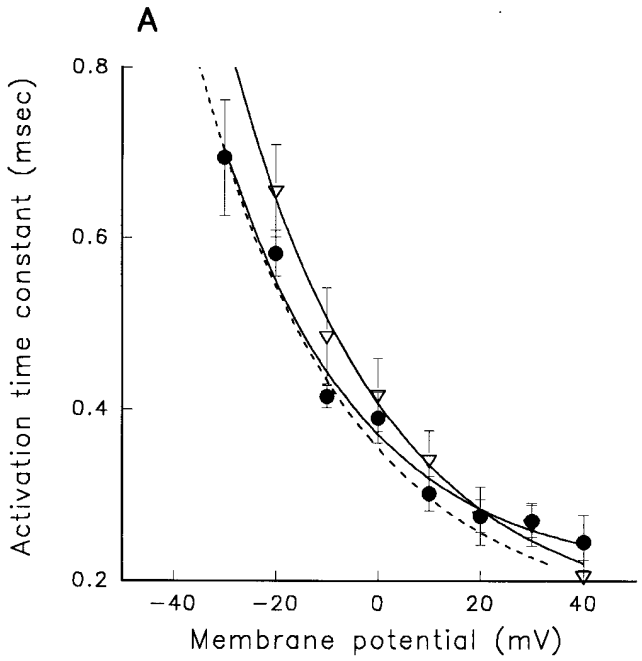

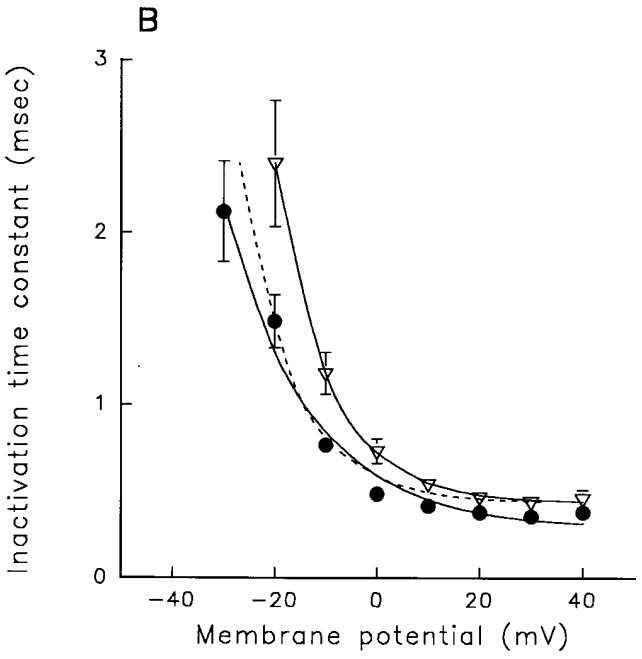

FIGURE 7. The kinetics of rSkM1 gating are altered in *lec2* cells. *Filled circles:* parent (wild-type) *pro5* rSkM1 currents; *open triangles:* sialylation-deficient *lec2* rSkM1 currents. Points are means ± SEM. Curves are fits of the data to single exponential functions. Time constants were measured as described in MATERIALS AND METHODS. (*A*) Time constants of activation for rSkM1 expressed in *pro5* and *lec2* cells. Broken line shows fit of activation time constants for *lec2* channels following a −7-mV shift along the voltage axis ($n = 6$ for *pro5* and *lec2* groups). (*B*) Time constants of inactivation for rSkM1 expressed in *pro5* and *lec2* cells. Broken line shows fit of inactivation time constants for *lec2* channels following a −7-mV shift along the voltage axis ($n = 6$ for *pro5* and *lec2* groups).

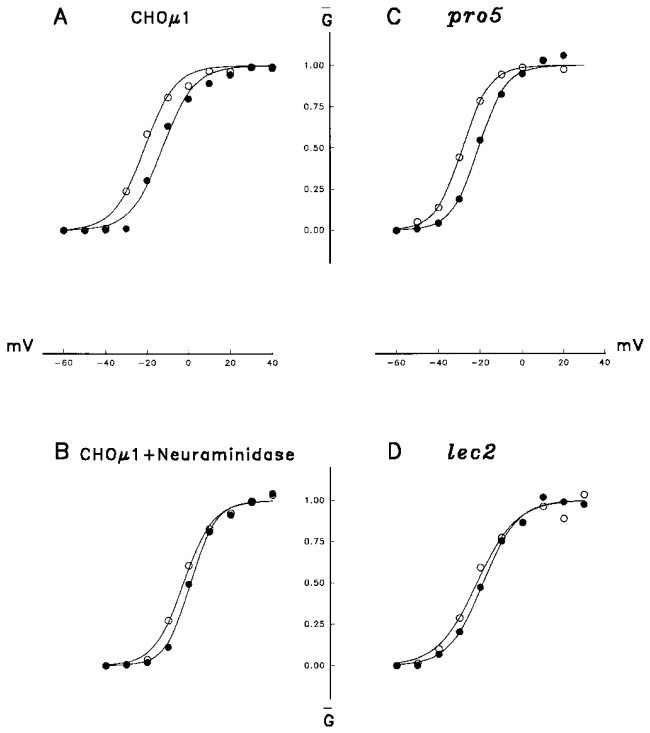

FIGURE 8. The effect of external calcium on steady state activation of rSkM1 is diminished under conditions of reduced sialylation. G-V relationships for rSkM1 as expressed in four different cell lines under two different external calcium concentrations for each. *Filled circles:* 2 mM calcium; *open circles:* 0.2 mM calcium (*A* and *B*) or 0.5 mM calcium (*C* and *D*). Points are means of three experiments (two for *pro5* data). Lines are fits of the data to single Boltzmann distributions. ΔV denotes the average difference in V_a ± SEM between calcium concentrations. (*A*) Untreated CHOμ1 cells, ΔV = 9.2 ± 0.6 mV. (*B*) CHOμ1 cells treated with neuraminidase, ΔV = 3.5 ± 0.8 mV. (*C*) *pro5* cells, ΔV = 7.7 ± 0.5 mV. (*D*) Sialylation-deficient *lec2* cells, ΔV = 2.4 ± 0.7 mV.

type molecule, respectively (Fig. 10 *A*, *inset*), with little difference between the corresponding bands of the two mutant forms.

Fig. 10 shows that steady-state activation and inactivation gating curves of these deletional mutants are shifted toward positive potentials. The magnitude of these shifts tend to be slightly smaller than those observed for either enzymatic or biosynthetically based reductions, consistent with the existence of a small amount of sialylation remaining on some of the other consensus sites present in the mutants (Table I).

Voltage gating behavior in these mutant channels was explored in detail in further tests of the electrostatic hypothesis. In particular, rates of activation and deactivation were determined in the absence of inactivation, which had been removed by proteolytic treatment (MATERIALS AND METHODS). As a result of this treatment, steady-state activation gating in both wild type and the mutants shifted by about 10 mV (Fig. 11).

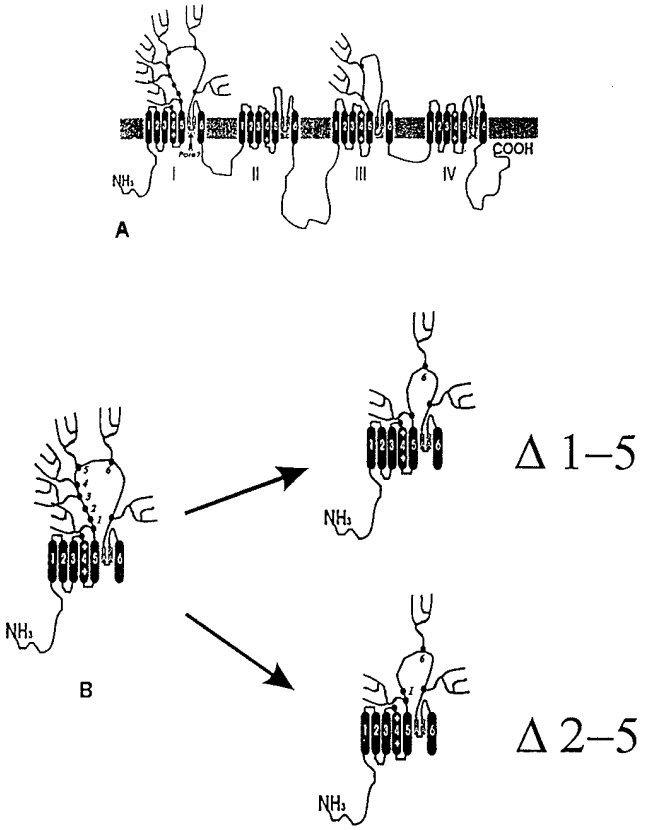

FIGURE 9. Schematic of rSkM1 and mutant clones. (*A*) Schematic of predicted secondary structure of rSkM1. The semi-homologous domains are labeled I-IV. Putative transmembrane spanning regions are labeled S1-S6. The pore forming regions are labeled A1 and A2. Potential sites of N-glycosylation are demarcated with a dot. Some sites are shown arbitrarily to be unglycosylated, as it is currently uncertain whether all are indeed modified either in CHO cells or native tissue. (*B*) Schematic illustrating the deletion constructs made. The left side is an enlargement of Domain I from *A*. Some of the potential N-glycosylation sites within the mutated loop are numbered arbitrarily for identification. The right side of the panel shows which sites were removed. As numbered, sites 1–5 and 2–5 were deleted for Δ1-5 and Δ2-5, respectively, resulting in a 30 mer and 24 mer deletion in this loop.

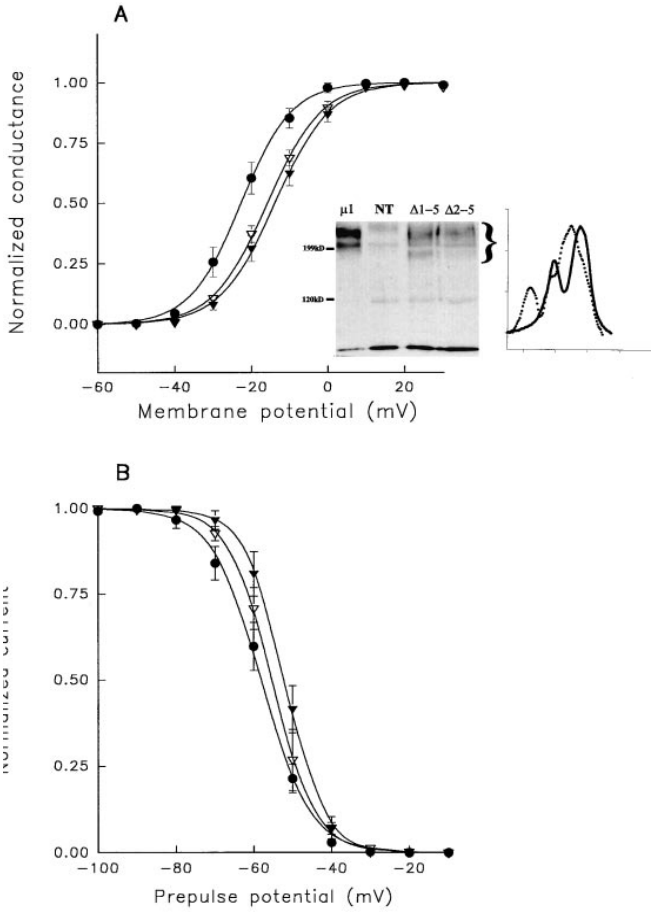

FIGURE 10. The voltage-dependence of steady-state gating of rSkM1 deletion mutants Δ1-5 and Δ2-5 is altered similarly to rSkM1 expressed under conditions of reduced sialylation. *Filled circles:* CHOμ1 (n = 10). *Open triangles:* Δ1-5 (n = 10). *Filled triangles:* Δ2-5 (n = 9). Points are means ± SEM and curves are fits of the data to single Boltzmann distributions. (*A*) G-V relationship. *Inset* (*left*): Western blot of cell extracts of CHO-μ1, nontransfected CHO (*NT*), and CHO lines transfected with Δ1-5 and Δ2-5 rSkM1 deletion mutants. *Inset* (*right*): Densitometric scans of major band region (*bracket on blot*) of CHO-μ1 (*solid trace*) and Δ1-5–transfected cells (*broken trace*), scaled as in Fig. 4. Densitometric scan of Δ2-5 lane was nearly identical to scan of Δ1-5 (not shown). (*B*) Steady state inactivation.

Such changes upon inactivation removal have been noted previously in certain other systems and have been interpreted as reflecting errors in estimating the fraction of open channels in the presence of inactivation when the inactivation rate is fast relative to the rate of activation (e.g., see Hille, 1992).

Regardless, in the present studies the relative shifts between wild-type and mutant channel gating were very similar to those seen for channels with intact inactivation (Fig. 11). This shows that the steady-state shifts described above under reduced sialylation conditions were not likely caused by differences in the influence of inactivation on measurement of the peak currents used to determine the conductance-voltage relations.

As seen with other means of reducing sialylation, the gating kinetics of channel mutants were shifted significantly toward positive potentials (Figs. 12 and 13). Thus activation, deactivation, and inactivation time constants of both mutant channels were shifted by 7–10 mV. Overall, then, the N-linked glycosylation mutant channels showed rather similar voltage shifts in gating behavior to other means of generally reducing glycosylation.

As with the other means of manipulation, the effects of both calcium and μ-conotoxin were determined for mutant channels. Thus the effect of external calcium concentration was also found to be significantly re-

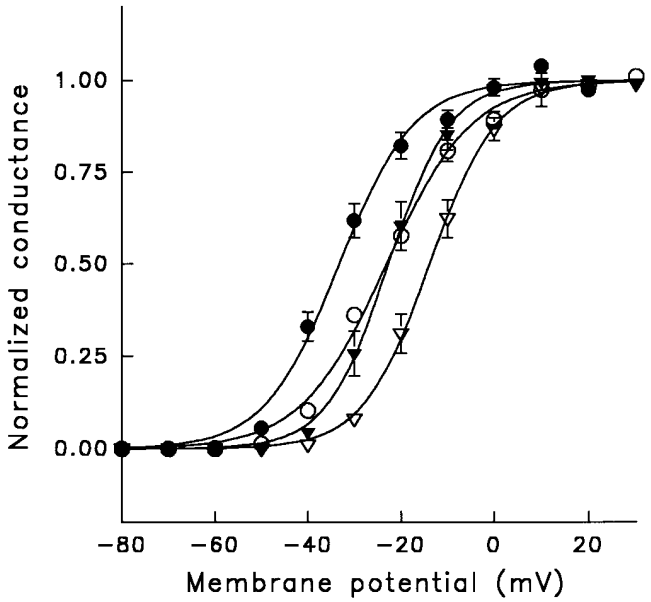

FIGURE 11. Inactivation removal does not effect the relative shift in steady-state activation between wild-type and mutant rSkM1 channels. Steady-state activation of rSkM1 and Δ2-5 in the presence and absence of inactivation. Data are the mean ± SEM conductance at a membrane potential. Curves are fits of the data to single Boltzmann distributions. *Open circles:* rSkM1, inactivation present ($n = 10$). *Open triangles:* Δ2-5, inactivation present ($n = 9$). *Filled circles:* rSkM1, inactivation removed ($n = 10$). *Filled triangles:* Δ2-5, inactivation removed ($n = 10$).

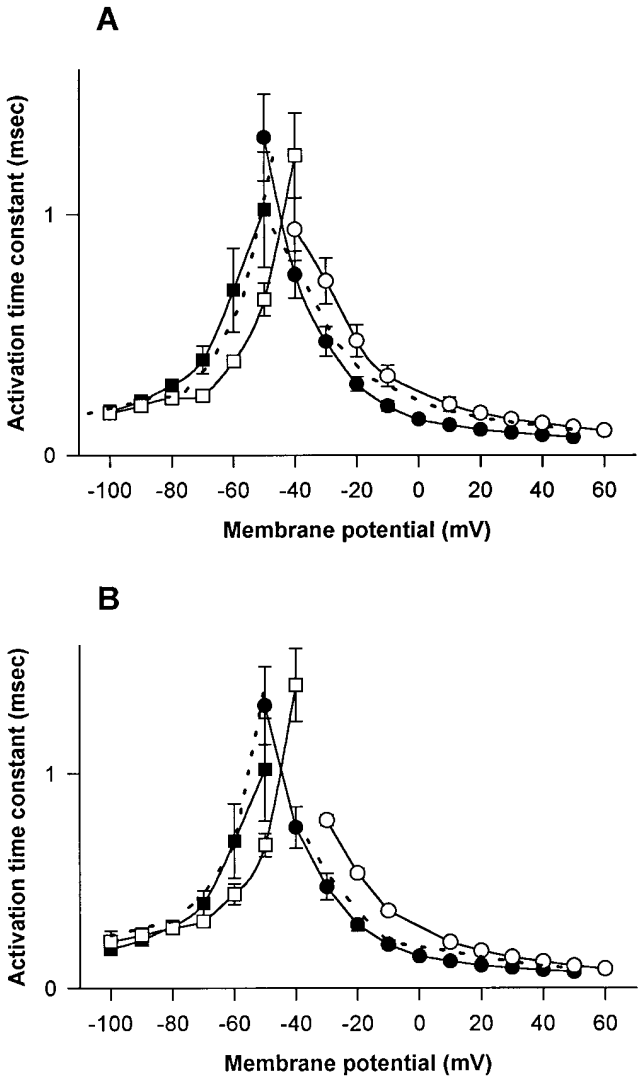

FIGURE 12. Mutant channel activation gating kinetics are shifted in the same direction and with similar magnitude as steady-state gating parameters. Time constants of activation and deactivation as functions of membrane potential. Data are mean ± SEM time constants at a membrane potential. Circles represent time constants of channel activation. Squares represent time constants of channel deactivation. Lines are nontheoretical point-to-point. Broken lines represent the deletion mutant data shifted by the same magnitude observed for shifts in steady state activation for the same mutant (Table I). (*A*) *Filled symbols:* rSkM1 ($n = 6$). *Open symbols:* Δ1-5 ($n = 8$). Broken line represents mutant data shifted by 7 mV. (*B*) *Filled symbols:* rSkM1 ($n = 6$). *Open symbols:* Δ2-5 ($n = 8$). Broken line represents mutant data shifted by 10 mV.

duced in the mutant channels ($P < 0.01$), although like other parameters, the magnitude of the effect was somewhat less than seen for the more general means of reducing sialylation described above (Fig. 14).

The inhibitory action of μ-conotoxin appeared unaffected by the removal of potential glycosylation sites (Fig. 15). Reversal potentials in these mutants were also unaltered, suggesting that the deletions of 24–30 amino acids had no discernible effect on selectivity properties of the channel, despite their relative proximity to domain "SS1-SS2" thought to be crucial to pore formation and ion selectivity (Heinemann et al., 1992). These results indicate that the deletions did not cause gross local conformation changes that might have affected channel gating allosterically.

DISCUSSION

The Voltage Dependence of Channel Gating Is Altered by Reducing Channel Sialylation

The data presented here show that three independent means expected to reduce sodium channel sialylation result in significant and similar changes to the voltage dependence of sodium channel gating. In particular, these manipulations resulted in depolarized displacements along the voltage axis of all the steady-state and kinetic gating relationships measured. How well do these observations agree with a model in which sialic acid contributes to a negative membrane surface potential and hence reduces the transmembrane field in the vicinity of channel gating elements?

In the simplest case, sialic acid residues would be evenly spread around the outside surface of the channel, and the manipulations used would have removed

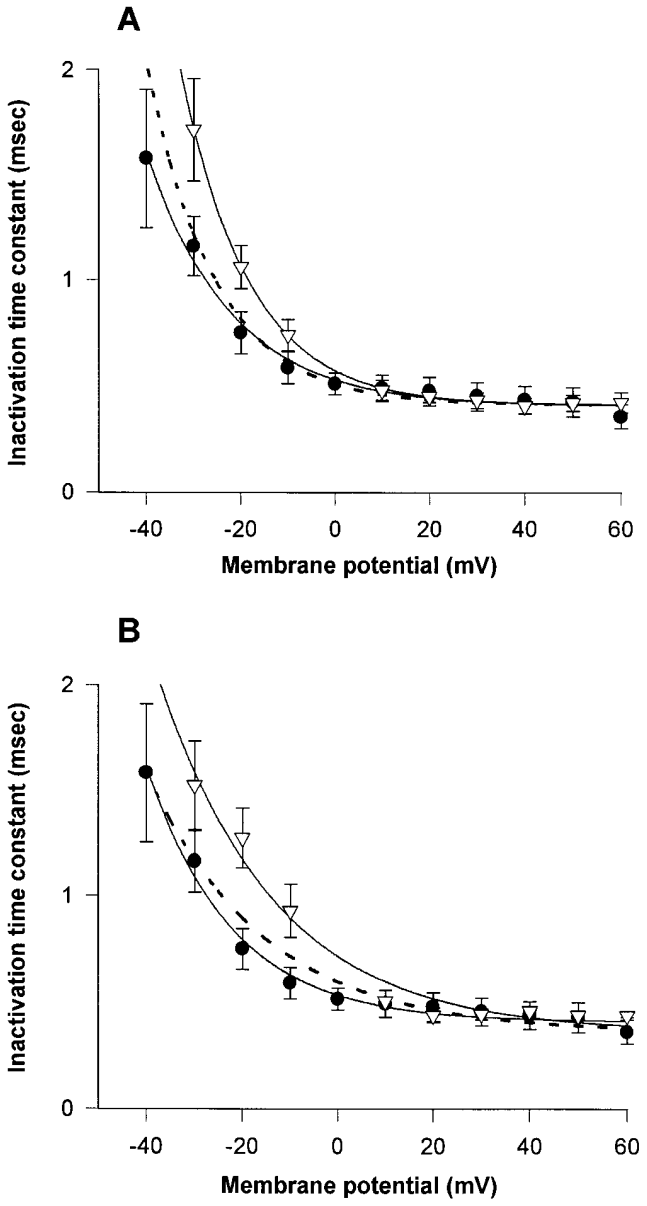

FIGURE 13. Inactivation gating kinetics shift similarly to activation gating kinetics. Time constants of channel inactivation as functions of membrane potential. Data are mean ± SEM time constants at a membrane potential. Solid curves are fits of the data to single exponential functions. Broken lines are fits of the mutant data to single exponentials following a 7- or 10-mV shift as described in Fig. 12. (*A*) *Filled circles:* rSkM1 ($n = 6$). *Open triangles:* Δ1-5 ($n = 8$). Broken line represents fit of mutant data to single exponential following a 7-mV shift. (*B*) *Filled circles:* rSkM1 ($n = 6$). *Open triangles:* Δ2-5 ($n = 8$). Broken line represents fit of mutant data to single exponential following a 10-mV shift.

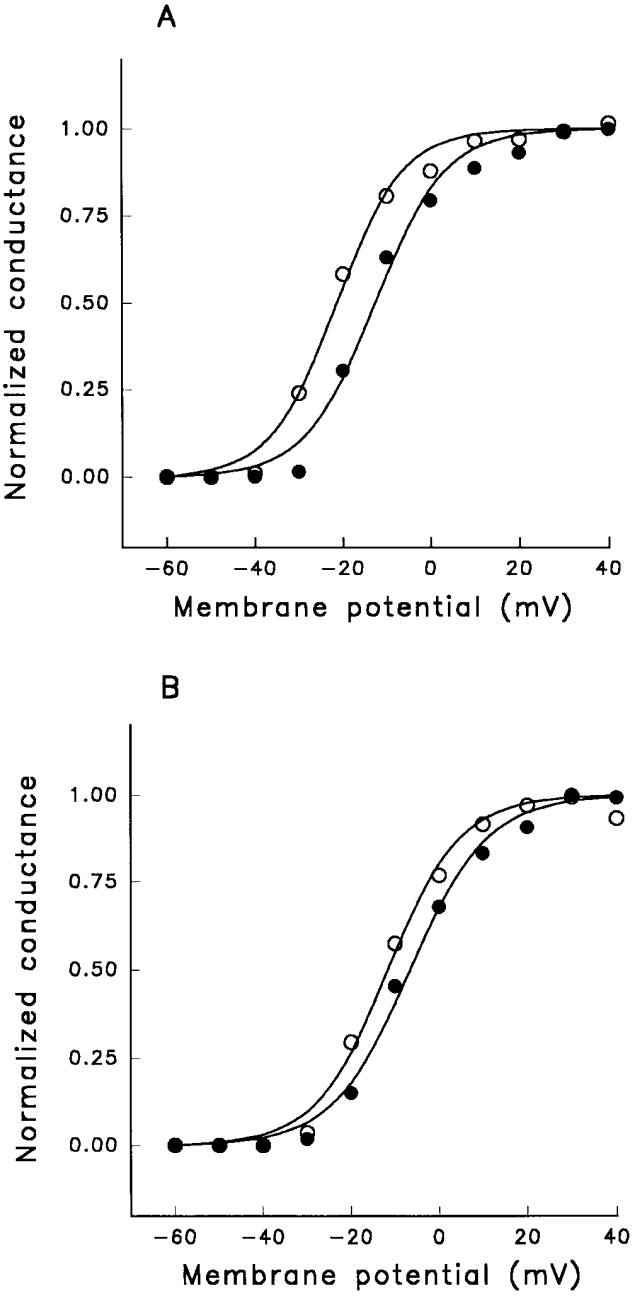

FIGURE 14. Mutant channel steady state activation is less affected by external calcium levels. Steady-state activation of rSkM1 and Δ2-5 at two different external calcium concentrations. Data are the mean conductance at a membrane potential. *Filled circles:* Conductance at 2.0 mM external calcium. *Open circles:* Conductance at 0.2 mM external calcium. ($n = 3$ for all data). Curves are fits of the data to single Boltzmann distributions. Average difference in V_a between calcium concentrations was 9.2 ± 0.6 mV for rSkM1 (*A*) versus 5.2 ± 0.7 mV for Δ2-5 (*B*).

sialic acids evenly and completely. If both these conditions hold, then the electrostatic paradigm might predict that shifts in the voltage dependence of gating would be similar in direction and magnitude for all gating parameters, and they would be the same regardless of the method used to decrease the level of sialylation.

How well do our results fit this simplified prediction? All comparisons of gating behaviors (steady state and kinetic) showed depolarizing shifts in voltage sensitivity under conditions expected to decrease channel sialyla-

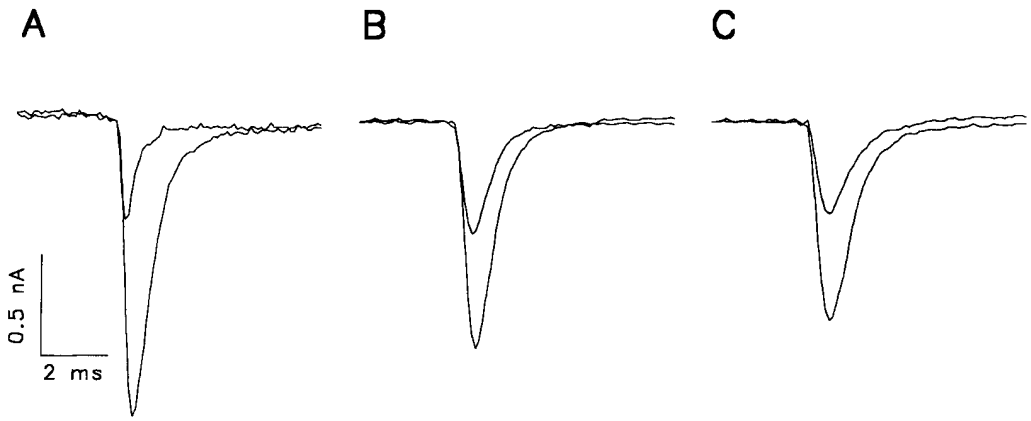

FIGURE 15. rSkM1 and the two mutant channels are similarly sensitive to μ-conotoxin. Traces are whole cell currents measured during a 9-ms pulse to −10 mV before and after the administration of 50 nM μ-conotoxin. Percentage inhibition ranged from 53 to 60%. (*A*) rSkM1; (*B*) Δ1-5; (*C*) Δ2-5.

tion (although two of these differences did not attain statistical significance; Table I). Quantitatively, shifts in a given gating behavior were very similar regardless of whether enzymatic means, sialylation-deficient CHO cells, or glycosylation site mutagenesis were used to reduce channel sialylation. Also, the sensitivity of channel activation to calcium shifts was shown to be reduced under conditions of lowered sialylation. Lastly, the magnitude of shifts induced by calcium under control conditions were similar to those seen with reduced sialylation, providing additional evidence that channel associated sialic acid residues are major sites of calcium interaction or screening as classically described. Overall, then, these results are generally consistent with the predictions of a simple model in which spatially homogenous sialylation more or less uniformly affects the electric field around voltage-sensitive gating elements of the sodium channel.

Evaluation of Other Mechanisms

On the other hand, the slope of the Boltzmann fits to the steady-state data decreased modestly as a result of sialic acid reduction by enzymatic or biosynthetic manipulation (as reflected in increases in the Z parameter, Table I). Classically, such effects could be interpreted to reflect intrinsic changes in the "effective valence" of a gating sensor, and as such might be taken as an indication that mechanisms other than electrostatic are responsible for the gating alterations observed. However, the slope changes are probably caused by small increases in gating heterogeneity arising from a population of channels with greater variations in sialylation, resulting in a broadened voltage range of activation and a shallower slope to the observed steady-state curves (for further discussion see Recio-Pinto et al., 1990). This view is supported by the smaller changes in Z seen in the deletion mutants, where due to absolute removal of glycosylation sites such heterogeneity should have been reduced. In any case, the contribution of the observed slope changes to apparent shifts in the steady-state curves was minor. Additionally, the shapes of the kinetic relations did not appear to change noticeably, as the curves obtained under reduced sialylation overlay the control data reasonably well (e.g., see dotted lines in Figs. 5, 7, 12, and 13). Overall, the manipulation of sialylation in these experiments appeared primarily to cause pure shifts of the gating relations along the voltage axis, as expected from a general change in the electric field around channel gating structures.

For rSkM1 in CHO cells, our data suggest that sialylation shifts voltage-dependent gating behavior by ~10 mV in the negative direction under physiological ionic and divalent conditions. One might ask whether the magnitude of such shifts is to be expected for charges on the outside of a channel molecule. While the actual location of sialic acid residues on sodium channels relative to gating voltage sensors is not presently known, in theory a single negative charge located at the extracellular surface of the cell membrane could reduce the transmembrane field by about 10 mV at a point ~15Å distant within the bilayer, well within the range of postulated gating elements such as the S4 motif (see Hille, 1992). Even if the sugars were located some distance away from the membrane surface, smaller additive effects from the large number of sialic acid residues present on a channel could combine to produce influences on the transmembrane field of this magnitude.

Two additional points might be considered here. First, one might ask whether indirect conformational consequences of desialylation could alternatively explain such changes in gating (see INTRODUCTION). The experiments presented here cannot definitively rule out such a mechanism; however, in general it might be expected that structural distortions would not produce such uniform changes in gating, particularly since the manipulations used to reduce channel glycosylation varied and thus altered channel carbohydrate structure differently. As such, effects of carbohydrate conformation on channel gating would not be bound by electro-

static influences and might result in either depolarizing or hyperpolarizing shifts in voltage sensitivity. In addition, these shifts might well affect various gating parameters very differently. In any case, we failed to detect changes in other characteristics (i.e., toxin inhibition, ion selectivity) mediated by amino acid segments fairly close to sites of N-glycosylation targeted by our manipulations.

Second, our simplifying assumptions regarding the spatial and functional uniformity of sialylation need not be correct for an electrostatic mechanism to hold. In fact, in some cases it has been found that changing external calcium concentration causes nonequivalent shifts on the voltage dependence of parameters describing channel function. (e.g., Frankenhaeuser and Hodgkin, 1957). If sialic acid residues are heterogeneously distributed and if different channel gating domains lie in different parts of the resulting nonuniform transmembrane electric field, then one would expect differential effects on particular gating behaviors which could depend on the means of sialic acid manipulation.

The Effects of Sialylation May Be Significantly Larger for rSkM1 Channels in Skeletal Muscle Fibers

The M_r decrease observed with neuraminidase treatment of rSkM1-transfected CHO cells (4.7 k) is much less than that seen for neuraminidase-treatment of skeletal muscle (~25 k). This suggests that the sialylation of rSkM1 is substantially reduced in CHO cells relative to skeletal muscle fibers in vivo, where sodium channel sialylation has been shown biochemically to account for 11.7% of the channel mass (Roberts and Barchi, 1987). In fact, it has been shown in other studies that CHO cells have significantly reduced sialylation capacities (due to lowered expression of certain sialyltransferases), resulting in reduced sialylation of endogenous membrane glycoproteins (Lee et al., 1989).

If rSkM1 channels in vivo are indeed more heavily sialylated than those studied here, then the electrostatic hypothesis would predict that in skeletal muscle the voltage-dependent gating of channels would occur at more hyperpolarized potentials and would exhibit a greater magnitude of calcium-induced shifts. This is the case, as sodium currents measured in physiological calcium in rat muscle fibers exhibit activation midpoints about 30 mV more negative than rSkM1 in wild-type CHO cells (Pappone 1980; Patel et al., 1994), while changes in external calcium shift steady state gating midpoints over a much greater range in muscle (54 mV) than in wild-type CHO cells (14 mV). These observations suggest that the high degree of sialylation of rSkM1 channels in skeletal muscle fibers affects sodium channel voltage sensitivity much more than apparently lower levels of sialylation in CHO cells (Patel et al., 1994).

Evidence That Sialylation Is Not Directly Involved in Trafficking and Insertion of rSkM1 Channels

If sialic acid were involved in either trafficking or insertion of channels, then the level of functional expression of the channel might be altered grossly in sialylation-deficient *lec2* cell lines or in cells transfected with the deletion channel mutants. Qualitatively, given the robust sodium currents observed in a significant fraction of these cells, it would seem that much of rSkM1 glycosylation is not absolutely required for biosynthesis and plasma membrane insertion of functional channels. In attempting to address this issue quantitatively using a large survey of cells, the levels of expression of rSkM1 in *lec2* and *pro5* cells were very similar (maximal sodium currents were 959 ± 139 pA [n = 37] for pro5 cells, 913 ± 113 pA [n = 29] for *lec2* cells), suggesting that lowered sialylation did not alter the number of functional channels in the membrane. However, these measurements cannot account for differences in transfection efficiency among various stably transfected cell lines, nor do they reflect the observation that among any given population of cells expression of current appears to be bimodal, with a significant fraction (50–75%) not expressing any measurable sodium current (see also variations in immunostaining, Fig. 1 *A*). At present one can only say that full glycosylation patterns are not necessary for functional expression of voltage gated sodium channels.

A Possible Physiological Role for Sialic Acid on Ion Channels

A possible physiological role for the effects of sialylation on channel activation might be to act as a regulator of activation voltage dependence. An inherent advantage could be gained by controlling voltage sensitivity in a channel through variable sialylation since such changes tend to preserve the properties of all voltage-sensitive phenomena relative to one another, shifting only the absolute voltage magnitude at which they occur. This phenomenon might be generalized to many voltage gated channels, as most are substantially sialylated. A recent study of Kv1.1 delayed rectifier potassium channels expressed in *lec* mutant cell lines shows similar effects of reduced sialylation on potassium channel gating (Thornhill et al., 1996). However, it is not possible at present to say whether gating modulation via sialylation occurs chronically or acutely in any cell system, or rather that channel gating structures have merely adapted to the presence of large numbers of sialic acid charges whose primary purpose is unrelated to voltage-dependent gating.

Other evidence of the functional importance of channel sialylation might be reflected in the symptoms affecting patients suffering from certain diseases that reduce protein glycosylation (Koscielik, 1995; Winchester

et al., 1995). Apart from perhaps reducing the number of functional channels, some of these disorders would be expected to reduce sodium channel sialylation, resulting in populations of channels that at rest lie further removed from the macroscopic threshold for action potential generation than normal. Such a situation could at least partially explain the neurological observations of reduced excitability, such as skeletal muscle weakness.

We would like to thank Dr. Gail Mandel for providing the rSkM1 clone and Eileen Mulvihill for providing the pZEM228 expression vector that were used throughout the study. Also, we would like to thank Drs. Kristin Schaller and Paul Fuchs for their advice and support during the initial stages of this project, and Drs. Angeles Ribera and William Sather for careful reading of the manuscript.

This work was supported by National Institutes of Health grants NS15879 (S.R. Levinson), NS09327 (E. Bennett), and NS07083 (E. Bennett).

Original version received 29 May 1996 and accepted version received 9 January 1997.

REFERENCES

Armstrong, C.M., and G. Cota. 1991. Calcium ion as a cofactor in Na channel gating. *Proc. Natl. Acad. Sci. USA.* 88:6528–6531.

Auld, V.J., A.L. Goldin, D.S. Krafte, W.A. Catterall, H.A. Lester, N. Davidson, and R.J. Dunn. 1990. A neutral amino acid change in segment IIS4 dramatically alters the gating properties of the voltage-dependent sodium channel. *Proc. Natl. Acad. Sci. USA.* 87: 323–327.

Campbell, D.T., and B. Hille. 1976. Kinetic and pharmacological properties of the sodium channel of frog skeletal muscle. *J. Gen. Physiol.* 67:309–323.

Chen, C.A., and H. Okayama. 1988. Calcium-phosphate-mediated gene transfer: A highly efficient transfection system for stably transforming cells with plasmid DNA. *Biotechniques.* 6:632–638.

Cota, G., and C.M. Armstrong. 1989. Sodium channel gating in clonal pituitary cells. The inactivation step is not voltage dependent. *J. Gen. Physiol.* 94:213–232.

Cukierman, S., W.C. Zinkand, R.J. French, and B.K. Krueger. 1988. Effects of membrane surface charge and calcium on the gating of rat brain sodium channels in planar bilayers. *J. Gen. Physiol.* 92: 431–447.

Dugandzija-Novakovic, S., A.G. Koszowski, S.R. Levinson, and P. Shrager. 1995. Clustering of Na^+ channels and node of Ranvier formation in remyelinating axons. *J. Neurosci.* 15:492–503.

Frankenhaeuser, B., and A.L. Hodgkin. 1957. The action of calcium on the electrical properties of squid axon. *J. Physiol. (Lond.).* 137:218–244.

Gordon, D., D. Merrick, D.A. Wollner, and W.A. Catterall. 1988. Biochemical properties of sodium channels in a wide range of excitable tissues studied with site directed antibodies. *Biochemistry.* 27:7032–7038.

Green, W.N, L.B. Weiss, and O.S. Andersen. 1987*a*. Batrachotoxin-modified sodium channels in planar lipid bilayers: ion permeation and block. *J. Gen. Physiol.* 89:841–872.

Green, W.N, L.B. Weiss, and O.S. Andersen. 1987*b*. Batrachotoxin-modified sodium channels in planar lipid bilayers: characterization of saxitoxin and tetrodotoxin-induced channel closures. *J. Gen. Physiol.* 89:873–903.

Hahin, R., and D.T. Campbell. 1983. Simple shifts in the voltage dependence of sodium channel gating caused by divalent cations. *J. Gen. Physiol.* 82:785–802.

Hamill, O.P., A. Marty, E. Neher, B. Sakmann, and F.J. Sigworth. 1981. Improved patch-clamp techniques for high-resolution current recording from cells and cell-free membrane patches. *Pflüg. Arch.* 391:85–100.

Heinemann, S.H., H. Terlau, W. Stuhmer, K. Imoto, and S. Numa. 1992. Calcium channel characteristics conferred on the sodium channel by single mutations. *Nature (Lond.).* 356:441–443.

Hille, B. 1992. Ionic Channels of Excitable Membranes. 2nd ed. Sinauer Associates, Inc. Sunderland, MA. 427–429.

Ivey, S., W.B. Thornhill, and S.R. Levinson. 1991. Monoclonal antibodies raised against posttranslational domains of the electroplax sodium channel. *J. Membr. Biol.* 121:215–222.

Koscielak, J. 1995. Diseases of aberrant glycosylation. *Acta Biochim. Pol.* 42:1–10.

Kraner, S., J. Yang, and R. Barchi. 1989. Structural inferences for the native skeletal muscle sodium channel as derived from patterns of endogenous proteolysis. *J. Biol. Chem.* 264:13273–13280.

Laemmli, U.K. 1970. Cleavage of structural proteins during assembly of the head of bacteriophage T4. *Nature (Lond.).* 227:680–685.

Lalik, P.H., D.S. Krafte, W.A. Volberg, and R.B. Ciccarelli. 1993. Characterization of endogenous sodium channel gene expressed in Chinese hamster ovary cell. *Am. J. Physiol.* 264:C803–C809.

Lee, E.U., J. Roth, and J.C. Paulson. 1989. Alteration of terminal glycosylation sequences on N-linked oligosaccharides of Chinese hamster ovary cells by expression of beta-galactoside alpha2,6-sialyltransferase. *J. Biol. Chem.* 264:13848–13855.

Messner, D.J., D.J. Feller, T. Scheuer, and W.A. Catterall. 1985. The sodium channel from rat brain: separation and characterization of subunits. *J. Biol. Chem.* 260:10597–10604.

Miller, J.A., W.S. Agnew, and S.R. Levinson. 1983. Principle glycopeptide of the tetrodotoxin/saxitoxin binding protein from *Elelctrophorus electricus.* Isolation and partial chemical and physical characterization. *Biochemistry.* 22:462–470.

Moczydlowski, E., B.M. Olivera, W.R. Gray, and G.R. Strichartz. 1986. Discrimination of muscle and neuronal Na-channel subtypes by binding competition between [^{3}H]-saxitoxin and μ-conotoxins. *Proc. Natl. Acad. Sci. USA.* 83:5321–5325.

Oxford, G.S. 1981. Some kinetic and steady-state properties of sodium channels after removal of inactivation. *J. Gen. Physiol.* 77:1–22.

Papazian, D.M., T.L. Schwarz, B.L. Tempel, L.C. Timpe, and L.Y. Jan. 1991. Ion channels in *Drosophila. Annu. Rev. Physiol.* 50:379–394.

Pappone, P.A. 1980. Voltage-clamp experiments in normal and denervated mammalian skeletal muscle fibres. *J. Physiol. (Lond.).* 306:377–410.

Patel, V.V. 1994. The contribution of nonprotein domains to the function of the voltage-dependent sodium channel. Ph.D. dissertation. Chapter 3. University of Colorado Health Sciences Center, University Microfilms, Ann Arbor, MI.

Patel, V.V., and S.R. Levinson. 1994. Calcium acts at multiple sites on skeletal muscle sodium channels. *Biophys. J.* 66:A103.

Patel, V.V., S.R. Levinson, and J.C. Caldwell. 1994. Surface charge variations account for the differences in gating of RSkM1 sodium channels in different cells. *Biophys. J.* 66:A102.

Recio-Pinto, E., W.B. Thornhill, D.S. Duch, S.R. Levinson, and B.W. Urban. 1990. Neuraminidase treatment modifies the function of electroplax sodium channels in planar lipid bilayers. *Neuron.* 5:675–684.

Roberts, R.H., and R.L. Barchi. 1987. The voltage-sensitive sodium channel from rabbit skeletal muscle. Chemical characterization of subunits. *J. Biol. Chem.* 262:2298–2303.

Stanley, P. 1985. Membrane mutants of animal cells: rapid identification of those with a primary defect in glycosylation. *Mol. Cell Biol.* 5:923–929.

Stanley, P. 1989. Chinese hamster ovary cell mutants with multiple glycosylation defects for production of glycoproteins with minimal carbohydrate heterogeneity. *Mol. Cell Biol.* 9:377–383.

Stuhmer, W., W.F. Conti, H. Suzuki, X.D. Wang, M. Noda, N. Yahagi, H. Kubo, and S. Numa. 1989. Structural parts involved in activation and inactivation of the sodium channel. *Nature (Lond.).* 339:597–603.

Thornhill, W.B., M.B. Wu, X. Wu, P.T. Morgan, and J.F. Margiotta. 1996. Expression of Kv1.1 delayed rectifier potassium channels in Lec mutant Chinese hamster ovary cell lines reveals a role for sialidation in channel function. *J. Biol. Chem.* 271:19093–19098.

Trimmer, J.S., S.S. Cooperman, S.A. Tomiko, J. Zhou, S.M. Crean, M.B. Boyle, R.G. Kallen, Z. Sheng, R.L. Barchi, F.J. Sigworth, et al. 1989. Primary structure and functional expression of a mammalian skeletal muscle sodium channel. *Neuron.* 3:33–49.

West, J.W., T. Scheuer, L. Maechler, and W.A. Catterall. 1992. Efficient expression of rat brain type IIA Na^+ channel α subunits in a somatic cell line. *Neuron.* 8:59–70.

Winchester, B., P. Clayton, N. Mian, E. di-Tomaso, A. Dell, A. Reason, and G. Keir. 1995. The carbohydrate-deficient glycoprotein syndrome: an experiment of nature in glycosylation. *Biochem. Soc. Trans.* 23:185–188.

Yang, N., and R. Horn. 1995. Evidence for voltage-dependent S4 movement in sodium channels. *Neuron.* 15:213–218.

Zhou, J., J.F. Potts, J.S. Trimmer, W.S. Agnew, and F.J. Sigworth. 1991. Multiple gating modes and the effect of modulating factors on the μl sodium channel. *Neuron.* 7:775–785.